INL/EXT-13-28750
Revision 0

RELAP-7: Demonstrating Seven-Equation, Two-Phase Flow Simulation in a Single-Pipe, Two-Phase Reactor Core and Steam Separator/Dryer

Ray Berry, Ling Zou, Haihua Zhao, David Andrs, John Peterson, Hongbin Zhang, Richard Martineau

April 2013

The INL is a U.S. Department of Energy National Laboratory
operated by Battelle Energy Alliance

INL/EXT-13-28750

RELAP-7: Demonstrating Seven-Equation, Two-Phase Flow Simulation in a Single-Pipe, Two-Phase Reactor Core and Steam Separator/Dryer

Ray Berry, Ling Zou, Haihua Zhao, David Andrs,
John Peterson, Hongbin Zhang, Richard Martineau

April 2013

Idaho National Laboratory
Idaho Falls, Idaho 83415

http://www.inl.gov

Prepared for the
U.S. Department of Energy
Office of Nuclear Energy
Under DOE Idaho Operations Office
Contract DE-AC07-05ID14517

EXECUTIVE SUMMARY

The RELAP-7 code is the next generation nuclear reactor system safety analysis code being developed at the Idaho National Laboratory. RELAP-7 will become the main reactor systems toolkit for the Risk-Informed Safety Margin Characterization Pathway of the Light Water Reactor Sustainability (LWRS) Program and the next generation tool in the RELAP reactor safety/systems analysis application series (i.e., the replacement for RELAP5). The code is being developed based on Idaho National Laboratory's modern scientific software development framework – MOOSE (i.e., the Multi-Physics Object-Oriented Simulation Environment).

The RELAP-7 thermal hydraulics systems analysis code employs a seven-equation, two-phase flow model, which treats each phase as being compressible and does not assume pressure equilibrium between phases. This physically motivated model exhibits full thermodynamic and mechanical nonequilibrium and has real characteristics, is well-posed, and is hyperbolic. Both phases are compressible to enable handling of wave propagation, bubble collapse, and other key phenomena occurring in light water nuclear reactors, either in normal or off-normal operation. An additional advantage of utilizing well-posed governing equations for multiphase flow is they can be strictly verified like any modern computational fluid dynamics models.

During the first half of Fiscal-Year 2013, the well-posed, seven-equation, two-phase flow model has been implemented into RELAP-7 via a seven-step process designed to progressively add additional physically- and numerically-meaningful models in self-contained steps of increasing complexity. This seven-step progression also allows for critical benchmark testing that pertains to each step, rather than the much more difficult task of trying to test specific phenomena after the complex model is built. Several major physical components, including a pipe ("Pipe"), a simple heated core channel ("Core Channel"), and a simple separator and dryer ("Separator/Dryer"), have been developed to support the demonstration calculations presented in this report. The cases selected for demonstration of the seven-equation, two-phase modeling in RELAP-7 include two-phase flow in a single pipe with and without wall heating, two-phase flow in one reactor core channel and two-phase flow in an small flow path with one core channel and steam separator.

In summary, the seven-equation, two-phase flow model has been implemented into the RELAP-7 code. The next major stage of development is to demonstrate two-phase flow modeling capability through a boiling water reactor loop and a simplified boiling water reactor station black out analysis, which will be reported in the subsequent demonstration simulation reports.

ACKNOWLEDGMENTS

Acknowledgement is made to the MOOSE team. Their close collaboration and support is essential to the success of this project. We would also like to acknowledge Stephen Hess and Greg Swindlehurst of EPRI for their valuable contributions to the development of the RELAP-7 application. Their expertise in nuclear engineering, systems analysis, and understanding of industry needs is much appreciated.

CONTENTS

EXECUTIVE SUMMARY v

ACKNOWLEDGMENTS vii

ACRONYMS xi

1. INTRODUCTION 1

2. SEVEN-EQUATION, TWO-PHASE FLOW MODEL 3

3. SIMULATION RESULTS 6

3.1 Variable Cross-Sectional Area Pipe Model 7

3.1.1 Case Study 1 7
3.1.2 Case Study 2 9
3.1.3 Case Study 3 10

3.2 A Two-Phase Flow Core Model 12

3.3 Steam Separator/Dryer Model 13

4. CONCLUSION AND FUTURE WORK 15

5. REFERENCES 16

Appendix A 17

FIGURES

Figure 1. Cross-sectional area of the converging-diverging pipe or flow channel. 8

Figure 2. RELAP-7 simulation results for the vapor phase under steady state, Case Study 1. 8

Figure 3. Simulation results for the liquid phase under steady state, Case Study 1. 9

Figure 4. Simulation results of Case Study 2, with strong phase interactions and relaxations: pressure (left), and velocity (right). 10

Figure 5. Simulation results of Case Study 2, with strong phase interactions and relaxations: shown are the phasic volume fractions. 10

Figure 6. Simulation results for Case Study 3, with wall heating: vapor volume fraction (left), and velocity (right) profiles. 11

Figure 7. Simulation results for Case Study 3 with wall heating, pressure (left), and temperature (right) profiles for both phases. 11

Figure 8. Schematic drawing of the core channel component model: fuel rod is in the center and is surrounded by coolant. 12

Figure 9. Simulation results for the vertical core channel component test: vapor volume fraction (left), and velocity (right) profiles. 13

Figure 10. Simulation results for the vertical core channel component test, pressure of both phases (left), and temperature profiles for both phases and fuel surface (right). 13

Figure 11. Schematic drawing of the steam separator/dryer component, connected with a two-phase core channel component, a water discharge pipe, and a steam outlet pipe. 14

TABLES

Table 1. Stiffened gas equation of state parameters for water and its vapor [10]. 6

Table 2. Summary of case studies, their descriptions, and implementation step from Appendix A. 7

Table 3. Mass and energy conservation between the steam separator/dryer inlet and outlets. 14

ACRONYMS

BWR	Boiling Water Reactor
DOE	Department of Energy
INL	Idaho National Laboratory
LWR	Light Water Reactor
MOOSE	Multi-Physics Object-Oriented Simulation Environment
RELAP5	Reactor Excursion and Leak Analysis Program 5
RELAP-7	Reactor Excursion and Leak Analysis Program 7

RELAP-7 Level 2 Milestone Report: Demonstrating Seven-Equation, Two-Phase Flow Simulation in a Single-Pipe, Two-Phase Reactor Core and Steam Separator/Dryer

1. INTRODUCTION

To simulate light water reactor (LWR) safety and design optimization scenarios, there are key issues that rely on in-depth understanding of basic, two-phase flow phenomena with heat and mass transfer. Within the context of these two-phase flows, two bubble-dynamic phenomena - boiling (or heterogeneous boiling) and flashing or cavitation (homogeneous boiling), with bubble collapse - are technologically very important. The main difference between boiling and flashing is that bubble growth (and collapse) in boiling is inhibited by limitations on the heat transfer at the interface, whereas bubble growth (and collapse) in flashing primarily is limited by inertial effects in the surrounding liquid. The flashing process tends to be far more explosive (or implosive) and is more violent and damaging (at least in the near term) than the bubble dynamics of boiling. However, other problematic phenomena [such as departure from nucleate boiling and CRUD (Corrosion Related Unidentified Deposit) deposition] are intimately connected with the boiling process. Practically, these two processes share many details and often occur together.

The state-of-the-art in two-phase modeling exhibits a lack of general agreement amongst the modeling technical community, even regarding the fundamental physical models that describe the complex phenomena. A large number of different models exist: homogeneous models, mixture models, two-fluid models, and drift-flux models are some examples. The various models have a different number of variables and a different number of describing equations; even the definition of the unknowns varies with similar models. There are conservative formulations, non-conservative formulations, models and techniques for incompressible flows, and for compressible flows. Huge Mach number variations can exist in the same problems - Mach number variations of 0.001 to over 10 with respect to mixture sound speed; high-speed versus low-speed gives way to the need for all-speed. In their recent compilation [1], Prospertti and Tryggvason made important statements that generally have been given insufficient attention in the past:

> *…uncertainties in the correct formulation of the equations and the modeling of source terms may ultimately have a bigger impact on the results than the particular numerical method adopted. Thus, rather than focusing on the numeric alone, it makes sense to try to balance the numerical effort with expected fidelity of the model.*
>
> *The formulation of a satisfactory set of average-equations models emerges as the single highest priority in the modeling of complex multiphase flows.*

Because of the expense of developing multiple special-purpose simulation codes and the inherent inability to couple information from these multiple, separate length and time scales physics, efforts at the Idaho National Laboratory (INL) have been focused toward development of multi-scale approaches to solve those multiphase flow problems relevant to LWR design and safety analysis. Efforts have been aimed at developing well-designed unified physical/ mathematical and high-resolution numerical models for compressible, all-speed multiphase flows spanning:

(1) well-posed general mixture level (true multiphase) models for fast transient situations and safety analysis,

(2) direct numerical simulation-like models to resolve interface-level phenomena (like flashing and boiling flows) and critical heat flux determination, and

(3) multi-scale methods to resolve (1) and (2) automatically, depending on specified mesh resolution, and to couple different flow models (e.g., single-phase, multiphase with several velocities and pressures or multiphase with single velocity and pressure).

In other words, we are extending the necessary foundations and building the capability to simultaneously solve fluid dynamic interface problems and multiphase mixtures arising from boiling, flashing of superheated liquid, and bubble collapse in LWR systems. Our goal is to provide models that resolve interfaces for larger bubbles (direct numerical simulation- like) with single-velocity, single-pressure treatment (interface capturing), and average (or homogenize) the two-phase flow field for small bubbles with two-velocity, two-pressure well-posed models.

The primary, enabling feature of the INL advanced multi-scale methodology for multiphase flows involves the way in which we deal with multiphase mixtures. This development extends the necessary foundations and builds the capability to simultaneously solve fluid dynamic interface problems and multiphase mixtures arising from boiling, flashing or cavitation of superheated liquid, and bubble collapse in LWR systems. Our multi-scale approach essentially solves the same equations everywhere with the same numerical method (in pure fluid, in multi-velocity mixtures, in artificially smeared zones at material interfaces, or in mixture cells, in phase transition fronts and in shocks). Some of the advantages of this approach include coding simplicity and robustness as a unique algorithm is used, conservation principles are guaranteed for the mixture, interface conditions are perfectly matched, and the ability to include the dynamic appearance/disappearance of interfaces. This method also allows the coupling of multi-velocities, multi-temperature mixtures to macroscopic interfaces where a single velocity must be present. This multi-scale methodology entails development on two main fronts. The first requires derivation (design) of theoretical models for multiphase and interfacial flows, whose mathematical description (equation system) is well-posed and exhibits hyperbolicity, exhibiting correct wave dynamics at all scales. The second requires design of appropriate numerical schemes to give adequate resolution for all spatial and time scales of interest.

Because of the broad spectrum of phenomena occurring in LWR coolant flows (e.g., boiling, flashing, bubble collapse, choking, blowdown, condensation, wave propagation, and large density variation convection), it is imperative that models accurately describe compressible multiphase flow with multiple velocities and that the models are well-posed and unconditionally hyperbolic. The currently popular, state-of-the-art, two-phase models assume the pressures in each phase are equal (i.e. they are single pressure models - referred to herein as the “classical” six-equation model). This approach leads to a system of equations that is ill-posed, not hyperbolic, and has imaginary characteristics (eigenvalues) that give the wrong wave dynamics. The classical six-equation model is inappropriate for many transient situations and is valid only for flows dominated by source terms (non-differential terms, such as interphase mass transfer, wall heat transfer, etc.). Numerical methods for obtaining the solution of the six-equation model rely on dubious properties of the numerical scheme (e.g., truncation error-induced artificial viscosity) to render them numerically well-posed over a portion of the computational spectrum. Thus, they cannot obtain grid-converged solutions (the truncation error goes down, thus the artificial viscosity diminishes and the ill-posed nature returns). This calls into question the possibility of obtaining “verification” and “validation” (what does it mean to validate a model that cannot be verified?).

To meet this criterion, we have adopted the seven-equation, two-phase flow model [2, 3, 4]. This equation system meets our requirements: as described above, it is hyperbolic, well-posed, and has a very

pleasing set of genuinely nonlinear and linearly degenerate eigenvalues[a]. This seven-equation system, which is described in the next section, is being implemented in RELAP-7 [5], via the INL's Multi-Physics Object-Oriented Simulation Environment (MOOSE) finite element framework [6]. This same seven-equation model, along with its reduced subsystems (see next paragraph), is being utilized as described above to build Bighorn, the next generation, three-dimensional, high-resolution, multi-scale single- and two-phase conjugate heat transfer solver. This will give a unique capability of consistently coupling the RELAP-7 system analysis code to our multidimensional, multi-scale, high-resolution multiphase solver and other MOOSE-based fuels performance packages.

There is yet another benefit to this approach that is alluded to above with the mention of the reduced subsystems of the seven-equation model. Because of the way the seven-equation system for two-phase flow is constructed, it can evolve to a state of mechanical equilibrium (phasic pressure and velocity equilibrium), whereby a very useful five-equation system results, and even further to thermodynamic equilibrium (phasic temperature and Gibb's energy equilibrium), whereby the classical three-equation homogeneous equilibrium model (HEM) results [7]. The rate at which these various equilibrium states are reached can be allowed to occur naturally or they can be controlled explicitly to produce a locally reduced model (reduced subsystem) to work with, or patch to, simpler models. For example, this reduction method enables the coupling of zones in which total or partial nonequilibrium effects are present to zones evolving in total equilibrium; or it can be used to examine the admissible limits of a physical system because all limited models are included in this general formulation.

2. SEVEN-EQUATION, TWO-PHASE FLOW MODEL

For the simulation of LWR coolant flows, general, two-phase flow models that allow velocity disequilibrium, but assume, or force, pressure equilibrium between the phases, typically have been used in the past (see Stadtke [8] for a recent review). These equations are usually ill-posed and not hyperbolic, exhibit incorrect wave dynamics, and they utilize solution algorithms that rely on questionable procedures such as truncation error induced artificial viscosity to render them numerically well-posed. Therefore, these traditional models cannot achieve a grid-converged solution because the truncation error (artificial viscosity) becomes small, allowing the ill-posed artifacts of the model to dominate. Well-posed, hyperbolic models are important for transient flows.

The RELAP-7 thermal hydraulics systems analysis code and companion multidimensional, two-phase conjugate heat transfer codes under development employ a seven-equation, two-phase model, which treats each phase as being compressible and does not assume pressure equilibrium between the phases. This physically motivated model exhibits full thermodynamic and mechanical nonequilibrium and has real characteristics, is well-posed, and is hyperbolic. Both phases must be compressible to handle wave propagation, bubble collapse, and other key phenomena occurring in LWRs (either in normal or off-normal operation). For more details of this model, refer to [9] and the references therein.

The fundamental components of this seven-equation model have been implemented as a one-dimensional, variable cross-sectional area system within RELAP-7 using the INL's MOOSE finite element framework. This will allow strong, seamless coupling with a growing family of neutronics, heat conduction, and fuels performance codes under development at INL, with all using the common MOOSE framework.

To facilitate implementation of this complex seven-equation model into the MOOSE framework, a logical sequence of steps was designed to begin with a simple compressible, single-phase model and then

[a] The seven wave speeds for the seven-equation model for two-phase compressible are the flow velocity for each phase, the forward- and backward-propagating phasic acoustic velocities relative to the flow velocity of each phase, and the interface velocity.

progressively add additional physically- and numerically-meaningful models in self-contained steps of increasing complexity. This 7-step progression also allows for critical benchmark testing pertaining to each step, rather than the much more difficult task of trying to test specific phenomena after the complex model is built. This is somewhat analogous to the need of orchestra members to tune their individual instruments separately, prior to their concert performance, during which such tuning would be much more difficult. The 7-step progression is documented in [9], which is included in Appendix A for completeness.

The basic seven-equation model for one-dimensional, compressible, two-phase flow in ducts of a spatially varying cross-sectional area consists of the following equations for each phase:

Volume Fraction Evolution

$$\frac{\partial \alpha_l A}{\partial t} + u_{\text{int}} A \frac{\partial \alpha_l}{\partial x} = A\mu(p_l - p_g) - \frac{\Gamma A_{\text{int}} A}{\rho_{\text{int}}} \tag{1}$$

$$\frac{\partial \alpha_g A}{\partial t} + u_{\text{int}} A \frac{\partial \alpha_g}{\partial x} = A\mu(p_g - p_l) + \frac{\Gamma A_{\text{int}} A}{\rho_{\text{int}}}$$
$$\left(\textit{not needed for } \underline{\textit{two}} \textit{ phases}, \alpha_g = 1 - \alpha_l\right) \tag{2}$$

Mass Balance

$$\frac{\partial \alpha_l \rho_l A}{\partial t} + \frac{\partial \alpha_l \rho_l u_l A}{\partial x} = -\Gamma A_{\text{int}} A \tag{3}$$

$$\frac{\partial \alpha_g \rho_g A}{\partial t} + \frac{\partial \alpha_g \rho_g u_g A}{\partial x} = \Gamma A_{\text{int}} A \tag{4}$$

Momentum Balance

$$\frac{\partial \alpha_l \rho_l u_l A}{\partial t} + \frac{\partial \alpha_l A(\rho_l u_l^2 + p_l)}{\partial x} = p_{\text{int}} A \frac{\partial \alpha_l}{\partial x} + p_l \alpha_l \frac{\partial A}{\partial x} + A\lambda(u_g - u_l) - \Gamma A_{\text{int}} u_{\text{int}} A$$
$$- f_l \alpha_l \rho_l \left(u_l - u_w\right)^2 \left(\pi A\right)^{\frac{1}{2}} - f_l' \tfrac{1}{2} \rho_l \left(u_l - u_{\text{int}}\right)^2 A_{\text{int}} A + \alpha_l \rho_l \vec{g} \cdot \hat{n}_{axis} A \tag{5}$$

$$\frac{\partial \alpha_g \rho_g u_g A}{\partial t} + \frac{\partial \alpha_g A(\rho_g u_g^2 + p_g)}{\partial x} = p_{\text{int}} A \frac{\partial \alpha_g}{\partial x} + p_g \alpha_g \frac{\partial A}{\partial x} + A\lambda(u_l - u_g) + \Gamma A_{\text{int}} u_{\text{int}} A$$
$$- f_g \alpha_g \rho_g \left(u_g - u_w\right)^2 \left(\pi A\right)^{\frac{1}{2}} - f_g' \tfrac{1}{2} \rho_g \left(u_g - u_{\text{int}}\right)^2 A_{\text{int}} A + \alpha_g \rho_g \vec{g} \cdot \hat{n}_{axis} A \tag{6}$$

Total Energy Balance

$$\frac{\partial \alpha_l \rho_l E_l A}{\partial t} + \frac{\partial \alpha_l u_l A(\rho_l E_l + p_l)}{\partial x} = p_{\text{int}} u_{\text{int}} A \frac{\partial \alpha_l}{\partial x} - \overline{p}_{\text{int}} A \mu (p_l - p_g) + \overline{u}_{\text{int}} A \lambda (u_g - u_l) + \Gamma A_{\text{int}} \left(\frac{p_{\text{int}}}{\rho_{\text{int}}} - H_{l\,\text{int}} \right) A + A_{\text{int}} h_{Tl} (T_{\text{int}} - T_l) A + \alpha_l h_{lw} (T_w - T_l) \left[4\pi A + \left(\frac{\partial A}{\partial x} \right)^2 \right]^{\frac{1}{2}} + \alpha_l \rho_l u_l \vec{g} \cdot \hat{n}_{axis} A \tag{7}$$

$$\frac{\partial \alpha_g \rho_g E_g A}{\partial t} + \frac{\partial \alpha_g u_g A(\rho_g E_g + p_g)}{\partial x} = p_{\text{int}} u_{\text{int}} A \frac{\partial \alpha_g}{\partial x} - \overline{p}_{\text{int}} A \mu (p_g - p_l) + \overline{u}_{\text{int}} A \lambda (u_l - u_g) - \Gamma A_{\text{int}} \left(\frac{p_{\text{int}}}{\rho_{\text{int}}} - H_{g\,\text{int}} \right) A + A_{\text{int}} h_{Tg} (T_{\text{int}} - T_g) A + \alpha_g h_{gw} (T_w - T_g) \left[4\pi A + \left(\frac{\partial A}{\partial x} \right)^2 \right]^{\frac{1}{2}} + \alpha_g \rho_g u_g \vec{g} \cdot \hat{n}_{axis} A \tag{8}$$

The first equation set is the volume fraction equation, the second is the mass balance equation, the third is the momentum balance, and the fourth is the total energy balance for each phase (i.e., liquid and vapor, respectively). Most of the two-phase nomenclature is standard, with additional terms as follows: A is the flow cross-sectional area, A_{int} is the interfacial area between the vapor and liquid per unit volume, p_{g} and p_{l} are the respective pressures of the vapor and liquid phase, p_{int} is the interfacial pressure, u_{int} is the velocity of the interface, and the mechanical relaxation parameters/functions are μ, the pressure relaxation function, and λ, the velocity relaxation function. Here, we take the interface variables as

$$u_{\text{int}} = \overline{u}_{\text{int}} + \text{sgn}\left(\frac{\partial \alpha_l}{\partial x} \right) \frac{p_g - p_l}{Z_l + Z_g}, \qquad \overline{u}_{\text{int}} = \frac{Z_l u_l + Z_g u_g}{Z_l + Z_g} \tag{9}$$

$$p_{\text{int}} = \overline{p}_{\text{int}} + \frac{Z_l Z_g}{Z_l + Z_g} \text{sgn}\left(\frac{\partial \alpha_l}{\partial x} \right) \cdot (u_g - u_l), \qquad \overline{p}_{\text{int}} = \frac{Z_g p_l + Z_l p_g}{Z_l + Z_g} \tag{10}$$

where $Z_k = \rho_k c_k \left(k = g, l \right)$ is the phasic acoustic impedance (where c_k is the phasic sound speed), and we choose the mechanical relaxation parameters as

$$\lambda = \frac{1}{2} \mu Z_l Z_g \quad \text{(velocity relaxation rate)} \tag{11}$$

$$\mu = \frac{A_{\text{int}}}{Z_l + Z_g} \text{ (pressure relaxation rate).} \tag{12}$$

For analytical expediency, we here employ the stiffened gas equation of state (SGEOS) for each phase

$$e(p,\rho)=\frac{p+\gamma p_\infty}{(\gamma-1)\rho}+q \qquad e(\rho,T)=c_v T+q+\frac{p_\infty}{\rho} \qquad c_p=\gamma c_v$$

$$\rho(p,T)=\frac{p+p_\infty}{(\gamma-1)c_v T} \qquad c^2=\frac{\gamma(p+p_\infty)}{\rho}=\gamma(\gamma-1)c_v T$$

$$h(T)=\gamma c_v T+q \qquad s(p,T)=c_v\ln\frac{T^\gamma}{(p+p_\infty)^{(\gamma-1)}}+q'$$

$$g(p,T)=h(T)-Ts(p,T)=(\gamma c_v-q')T-c_v T\ln\frac{T^\gamma}{(p+p_\infty)^{(\gamma-1)}}+q \tag{13}$$

where γ, q, and p_∞ are fluid properties, different for each phase. Table 1 gives the values used in our initial efforts.

Table 1. Stiffened gas equation of state parameters for water and its vapor [10].

Water	γ_k	$q_k\ (J\cdot kg^{-1})$	$q'_k\ (J\cdot kg^{-1}\cdot K^{-1})$	$p_{\infty k}\ (Pa)$	$c_{vk}\ (J\cdot kg^{-1}\cdot K^{-1})$
Liquid	2.35	$-1167\cdot10^3$	0	10^9	1816
Vapor	1.43	$2030\cdot10^3$	$-23\cdot10^3$	0	1040

Appendix A and references [2, 9] contain further details and descriptions of terms in these equations.

This set of equations is an initial, demonstration set to test the salient multiphase phenomenological effects. It is not a complete representation of all submodels and constitutive relations necessary to represent all of the diverse LWR coolant flows. For example, it does not include pressure differences that can be sustained due to relative velocity between the phases or due to surface tension. We refer to these sustained, steady state, or static pressure differences as *structural* or *configurational pressures* because they are due to the structure or configuration of the phases. These additional effects can be sustained at steady state; therefore, for very rapid volume fraction evolution, these residual force balances can become an algebraic closure relation. Such pressure differences can be accommodated, as appropriate, with modification of the volume fraction evolution equation and the interface pressure expressions in the momentum and energy equations. We have neglected these terms initially for clarity of presentation and retained only the fastest-evolving thermodynamic nonequilibrium terms. This initial system also does not include wall boiling/condensation or virtual mass effects. All such improvements are critical and will be added in the future, upon satisfactory testing of this initial model.

3. FLOW DEMONSTRATION RESULTS

As discussed in the previous section, the complex seven-equation model has been implemented in the RELAP-7 code in a logical sequence of steps, beginning with a simpler, single-phase compressible flow model and then progressively adding additional physics terms to complete the model. In this section, benchmark results for several key steps are provided to demonstrate the seven-equation model's capability in dealing with different complexity levels of two-phase flow simulation, from simple, single-phase compressible flow to more complex, two-phase flow with phase change due to wall heating.

3.1 Variable Cross-Sectional Area Pipe Model

The one-dimensional, 'pipe' component has been developed as one of the basic thermal-hydraulics analysis components in the RELAP-7 code. The isothermal (two-equation) and non-isothermal (three-equation), single-phase flow prediction capabilities have been implemented in the pipe component and reported in the last milestone report [5]. With the implementation of the seven-equation two-phase model, the pipe component has also been extended to handle variable cross-sectional area, including the case of constant pipe area as a special case.

To demonstrate the seven-equation capability with the pipe component of variable cross-sectional area, several benchmark results are provided in this section. It includes test cases: (1) two-phase flow in a pipe with converging-diverging cross-sectional area, while no phase interaction is present, (2) two-phase flow in a pipe with converging-diverging cross-sectional area, with phase interaction and relaxation both present, and (3) two-phase flow in a straight pipe with constant cross-sectional area, with phase change from wall heating. Table 2 summarizes a brief description of each of the three case studies along with the corresponding implementation step from Appendix A.

Table 2. Summary of case studies, their descriptions, and implementation step from Appendix A.

	Descriptions
Case study 1	Two phases coexist, no any interactions between phases (Appendix A, step 3)
Case study 2	Two phases coexist, interfacial phase interactions, velocity and pressure relaxations are included (Appendix A, step 5)
Case study 3	Two phases coexist, interfacial phase interactions, mass and heat transfers, velocity and pressure relaxations, wall heat transfer and friction, gravity effect, are all included (Appendix A, step 7)

3.1.1 Case Study 1

In this section, the simulation results are provided for the Case Study 1, two-phase flow in a pipe with converging-diverging cross-sectional area, while no phase interaction is present. In this test case, the two phases, liquid and vapor, coexist in the same pipe while there are no interactions between them (i.e., no interfacial velocity, pressure, and velocity relaxations and phase changes [Step-3 in Appendix A]). For this simulation a converging-diverging pipe 1 meter long was used, with inlet and outlet areas of 1.5 m^2 and a throat area of 0.5 m^2, and with cross-sectional area given by (shown in Figure 1)

$$A = 1.0 + 0.5\cos(2\pi x) \quad [m^2] \ . \tag{14}$$

The stagnation inlet boundary condition is specified on the left end of the pipe (x = 0) for both phases, with a stagnation pressure at 1.0 MPa and a stagnation temperature at 423.5 K. The inlet vapor void fraction is specified at 0.5 on the left boundary. The static outlet boundary condition is specified on the right end of the pipe (x = 1) for both phases, with a static pressure at 0.5 MPa. The transient simulation starts from initial conditions of constant static pressure at 0.5 MPa and static temperature at 423 K, in the entire simulation domain, and then converges to a steady-state solution. The RELAP-7 steady-state solution results are shown in Figure 2 and Figure 3 for vapor phase and liquid phase, respectively. As clearly shown in Figure 2, for the given inlet and outlet conditions, a shock is developed for the vapor phase at position $x \approx 0.8$. On the contrary, the liquid phase shows no shock in its steady-state solution using the same boundary conditions. It has to be noted that negative pressure values are obtained for liquid phase for this example, because the stiffened gas equation of state permits negative pressure as long as the sum of p and p_∞ remains positive (no phase change is permitted for this case). The resulting volume fraction solutions for both phases, which remain constant at 0.5 (as expected), are not shown here. The solution obtained with RELAP-7, including void fraction, pressure, density, velocity, and temperature for both phases agree well with the analytical solutions [2].

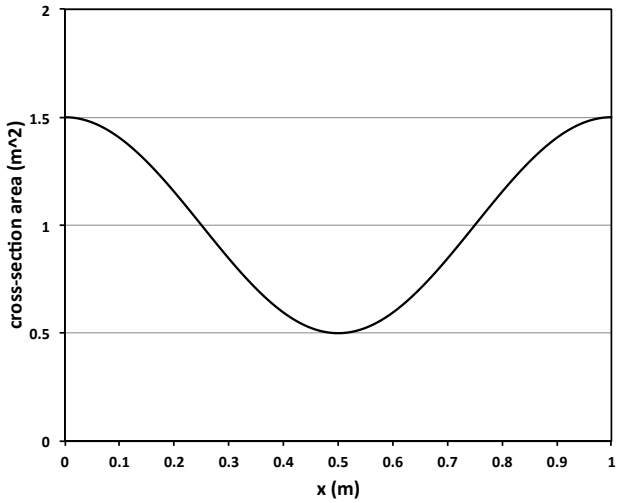

Figure 1. Cross-sectional area of the converging-diverging pipe or flow channel.

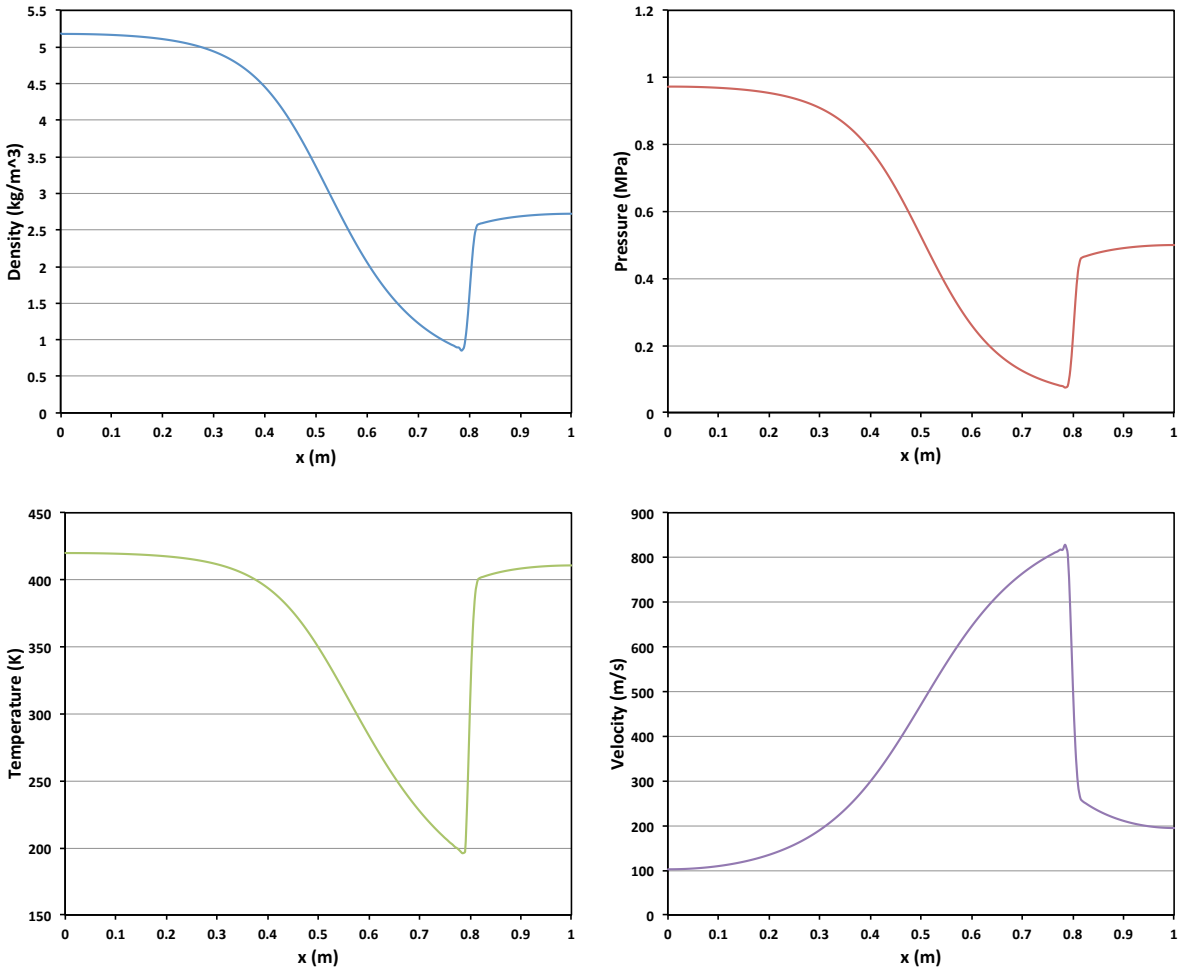

Figure 2. RELAP-7 simulation results for the vapor phase under steady state, Case Study 1.

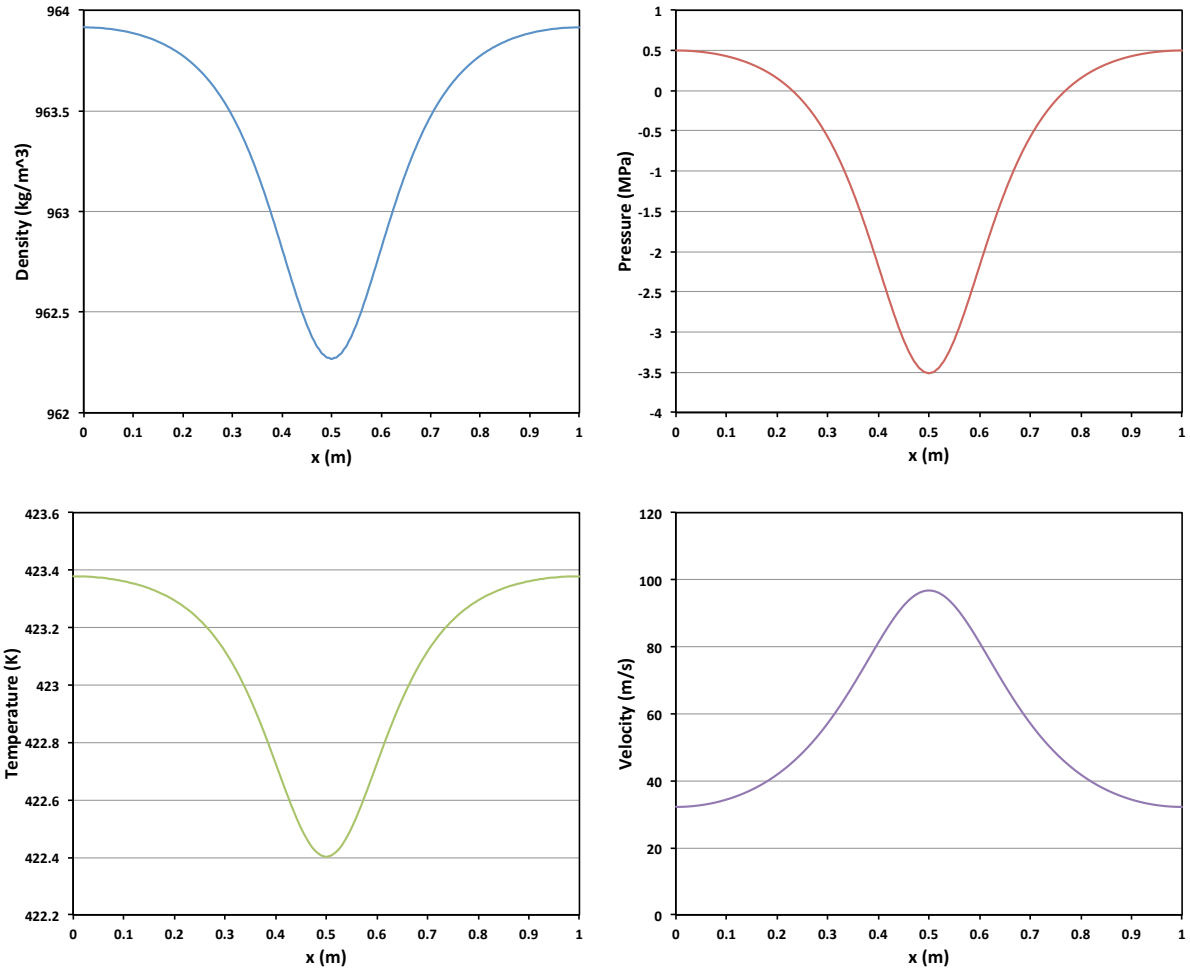

Figure 3. Simulation results for the liquid phase under steady state, Case Study 1.

3.1.2 Case Study 2

The simulation results of Case Study 2 are shown in Figure 4 and Figure 5. This simulation includes additional physics from that of Case Study 1. In this case, the pipe cross-sectional area and all initial and boundary conditions remain the same as those of Case Study 1. The difference is that the interfacial phase interaction, the strong pressure, and velocity relaxations are all included in this study (Step 5 in Appendix A). Figure 4 shows the pressure and velocity profiles for both phases along the pipe length. Because of the strong phase interaction and relaxations, the pressure (and velocity) of both phases exhibit almost the same profiles. Compared to Figure 3 of the Case Study 1 results, the liquid phase pressure in this case is no longer negative because the pressure tends to reach equilibrium between two phases due to the strong pressure relaxation. Similar to the velocity profile and due to the strong velocity relaxation between the two phases, the vapor velocity decreases dramatically from around 800 m/s in Case Study 1 to around 70 m/s in Case Study 2 in the shock region. Also, it should be noted that the shock developed in Case Study 2 is not as sharp as Case Study 1 due to the phase interactions. The void fractions of both phases are shown in Figure 5. In Case Study 1, the vapor phase has much higher pressures than the liquid phase because it is not allowed to expand against the liquid, i.e. the phase interactions are not present. In Case Study 2, the vapor phase expands and, therefore, occupies more volume (shown in Figure 5).

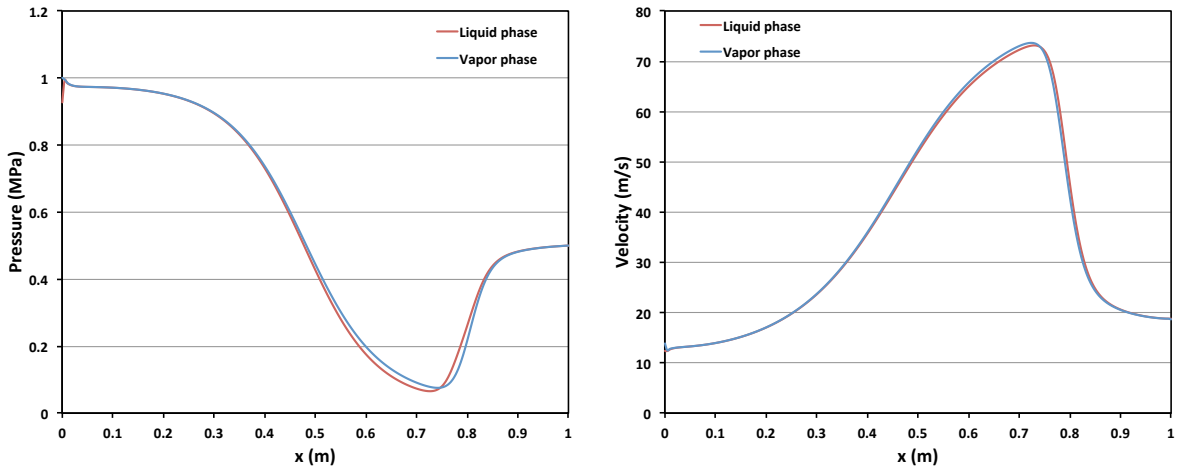

Figure 4. Simulation results of Case Study 2, with strong phase interactions and relaxations: pressure (left), and velocity (right).

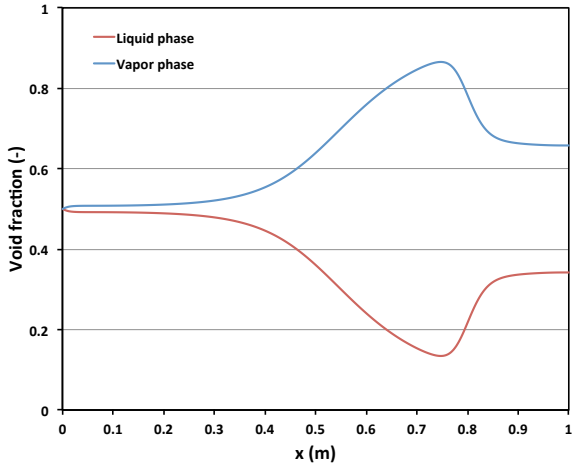

Figure 5. Simulation results of Case Study 2, with strong phase interactions and relaxations: shown are the phasic volume fractions.

3.1.3 Case Study 3

In this case study, interfacial heat and mass transfers (as well as wall heating effect), wall friction, and gravity effects are all included. In this case, the two-phase flow simulation takes place in a round, straight pipe with a constant cross-sectional area, 1.0×10^{-4} m^2. Static boundary conditions are applied on both the inlet and the outlet in this simulation. The inlet pressure and temperature are set at 0.505 MPa and 395.248 K, respectively. The outlet pressure is set at 0.5 MPa. The inlet vapor void fraction is set at 1.0×10^{-4} to represent a nearly pure liquid inlet condition. To generate vapor from phase change, heat is supplied from the wall to the fluids, with a constant wall temperature at 400 K, and a constant wall heat transfer coefficient at 1.5×10^4 W/m^2-K. Wall friction also is included to balance the pressure difference

between the inlet and the outlet. The pipe is oriented horizontally; therefore gravity has no effect in this simulation.

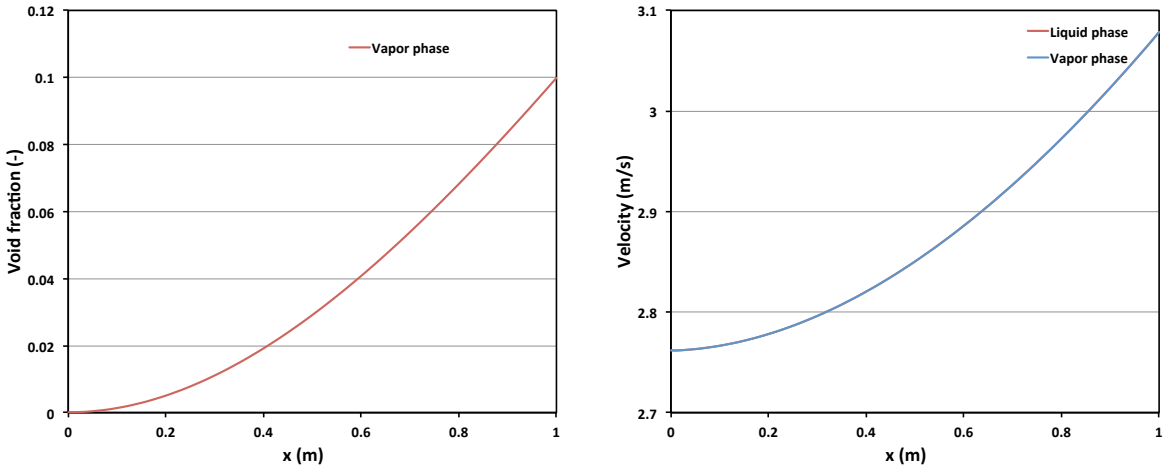

Figure 6. Simulation results for Case Study 3, with wall heating: vapor volume fraction (left), and velocity (right) profiles.

As shown in Figure 6, due to wall heating, the vapor void fraction increases along the pipe length as the two-phase flow travels through the pipe from left to right. The outlet vapor void fraction reaches a value around 10%. The temperature profiles of both phases are shown in Figure 7. The vapor temperature is close to the local saturation temperature (not shown), while the liquid temperature is slightly higher than the local saturation temperature. In other words, the liquid phase is superheated to support the phase change. The pressure profiles also are shown in Figure 7, with vapor pressure higher than the local liquid pressure. However, it should be noted that in realistic, two-phase boiling heat transfer within heated pipes, most of the phase change takes place on the wall rather than in the bulk region. In the future, such two-phase closure laws will be included to predict wall boiling heat transfer results.

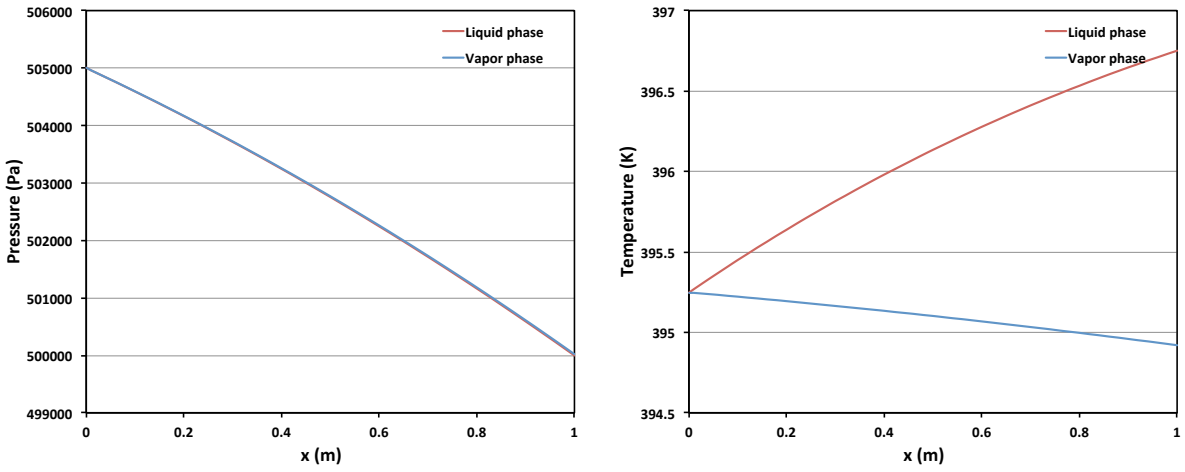

Figure 7. Simulation results for Case Study 3 with wall heating, pressure (left), and temperature (right) profiles for both phases.

3.2 A Two-Phase Flow Core Model

In this section, the two-phase flow, seven-equation model is implemented in the "core channel" component, with coupled, two-phase pipe flow and heat conduction in the fuel (schematically shown in Figure 8). The core channel component is implemented with separated pipe and heat structure components to implement the two-phase flow fluid equations (in the surrounding coolant) and heat conduction equation (in the fuel rod), respectively. The strongly coupled conjugate heat transfer between the fuel rod and the surrounding coolant is realized by nodal variable coupling between pipe mesh nodes and heat structure mesh nodes. The "core channel" component is used to represent a reactor core model.

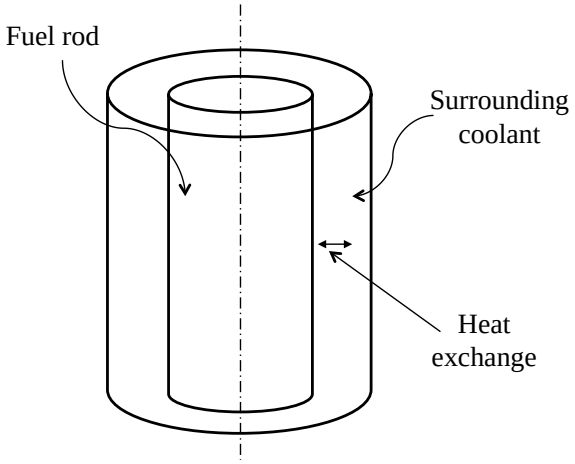

Figure 8. Schematic drawing of the core channel component model: fuel rod is in the center and is surrounded by coolant.

In this simulation, the vertical core channel is 1 m in length, with fuel rod diameter of 0.01 m, and the surrounding coolant flow area of 1.0×10^{-4} m^2. A total power of 3600 W with a sinusoidal profile is supplied in the fuel region. The inlet boundary conditions are applied at the bottom of the core channel component, with inlet static pressure at 0.513 MPa and inlet temperature at 395.771 K. The outlet static pressure is set at 0.5 MPa. The heat transfer coefficient is set as constant at 2.0×10^4 W/m^2-K. The simulation results of a two-phase flow core model are shown in Figure 9 and Figure 10. The steady-state outlet vapor void fraction is ~30% under the given boundary conditions and energy source. The liquid phase temperature is superheated to supply the phase change. As discussed in Section 3.1.3, to improve the simulation in the future, wall-boiling models will be added. It also should be noted that the pressure profiles of both phases exhibit slight oscillations near the inlet and outlet regions. It could be caused by the physical instability due to strong two-phase coupling or by numerical instability; the phenomenon is undergoing further investigation.

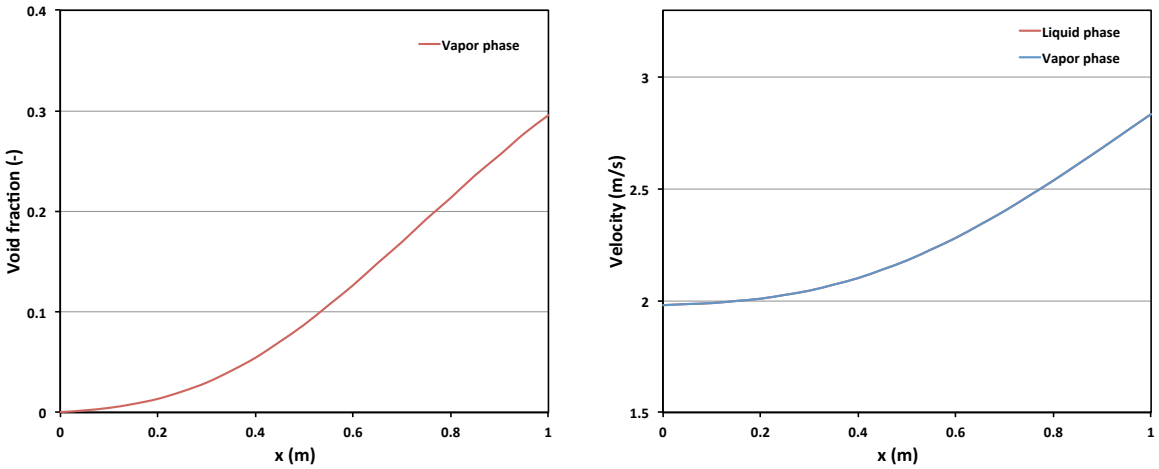

Figure 9. Simulation results for the vertical core channel component test: vapor volume fraction (left), and velocity (right) profiles.

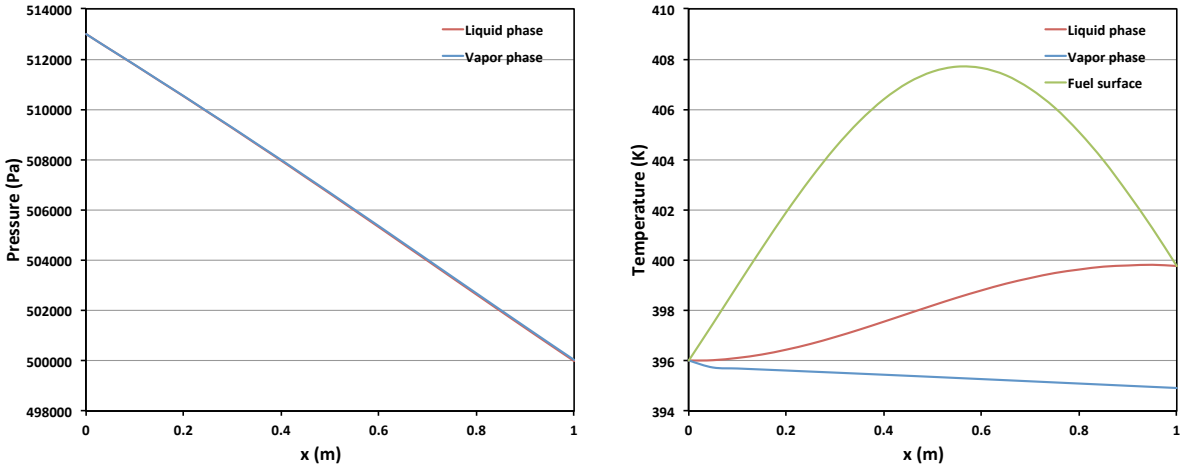

Figure 10. Simulation results for the vertical core channel component test, pressure of both phases (left), and temperature profiles for both phases and fuel surface (right).

3.3 Steam Separator/Dryer Model

In boiling water reactor (BWR) systems, the purpose of steam separators and steam dryers is to separate steam from the two-phase, steam-water mixture at the core outlet. After leaving the upper plenum, the two-phase, steam-water mixture enters (vertically) the steam separator assemblies. This mixture impinges on vanes and creates a vortical motion that generates centrifugal forces to separate the water from the mixture. In general, there are several stages of such a process in the steam separator assemblies. Eventually, the high-quality steam flow enters the steam dryer assembly, while the water drains back to the annular downcomer region. The high-quality steam enters the dryer assemblies, passing through chevron-type drying vanes to further remove moisture from the steam, reaching a steam quality higher than 99.99% [11].

No models are available in existing reactor system analysis codes to simulate, with first principles, the complex mechanisms of separating the two-phase mixture in either the steam separator or the steam dryer component. In the development of RELAP-7, we also do not intend to mechanistically predict the very complex mechanisms in the steam separator and the steam dryer. Both components serve the same purpose of separating almost pure steam from the two-phase mixture. These two components are combined as a single component in RELAP-7, as in most other existing systems safety analysis codes [11, 12]. An ideal separation condition is also assumed for steady-state simulation (i.e., the two-phase mixture is separated as pure water and pure steam from this combined steam separator/dryer component). In the separation process, mass and total energy are conserved from the inlet of the steam separator/dryer component to its two outlets (i.e., water discharge outlet and steam outlet).

In this simulation, a two-phase flow core channel component, a water discharge pipe, and a steam outlet pipe are connected with the steam separator/dryer component (schematic drawing shown in Figure 11). The parameters used for the two-phase, core channel component are the same as those presented in Section 3.2. The horizontal water discharge pipe and vertical steam outlet pipe are both set with 0.5 m in length and 1.0×10^{-4} m^2 in cross-sectional area. The analysis results are tabulated in Table 3. The comparisons of the mass and total energy flux between the inlet two-phase flow and the outlet flows show excellent balance between inlet and outlets, which indicates a steady-state, ideal, two-phase flow separation is achieved.

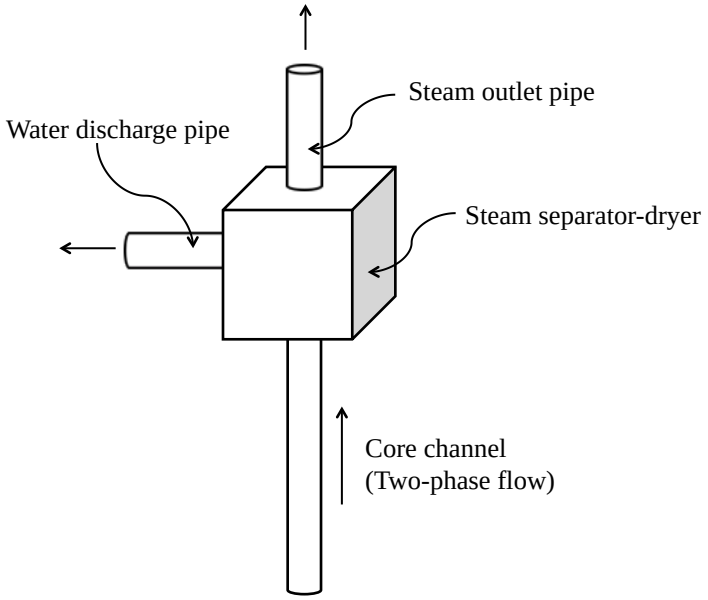

Figure 11. Schematic drawing of the steam separator/dryer component, connected with a two-phase core channel component, a water discharge pipe, and a steam outlet pipe.

Table 3. Mass and energy conservation between the steam separator/dryer inlet and outlets.

		Mass Flow Rate (kg/s)	Total Energy Flow Rate (W)
Inlet	Liquid phase	2.0386E-01	1.0979E+05
	Vapor phase	2.3737E-04	5.7934E+02
Outlets	Water discharge	2.0386E-01	1.0979E+05
	Steam outlet	2.3737E-04	5.7943E+02

4. CONCLUSION AND FUTURE WORK

The seven-equation, compressible two-phase flow model has been implemented successfully into the RELAP-7 code. Results were shown for a variable area pipe component, a two-phase flow core model, and a steam separator/dryer component. The next stage of development is to demonstrate the two-phase flow modeling capability for a BWR loop and a simplified BWR station blackout analysis, which will be reported in a future demonstration simulation report.

Though significant accomplishments have been achieved, much remains. Only simplified closures have been used in the demonstration calculations presented in this report. The term closures denotes any sub model (algebraic or differential) used to augment the information lost in the averaging of the conservation-law system model, e.g. interphase heat and mass transfer models along with their coefficient functions, topological interfacial area descriptions (flow regime maps), wall heat and mass transfer models, etc. Closures also denote any specific functional relationships necessary, in addition to the conservation-law system, necessary to endure a unique solution, e.g. equations of state to represent specific fluids. In addition to the descriptive model improvements discussed in the last paragraph of Section 2, future efforts include development of appropriate closure models for the seven-equation model. The seven-equation, two-phase flow model is different from the commonly used, two-fluid, six-equation models of existing safety analysis codes. Although many of the closure models used in the existing codes can be adapted for the seven-equation model, some additional model developments (e.g. equations of state) and experiments are expected to fully support the seven-equation model. A complete set of closure models for all of the important two-phase flow regimes must necessarily be implemented and validated before RELAP-7 can predict safety transients with much reduced uncertainty from that of existing codes. For example, it is well known that the current flow regime map-based method to select closure models for two-phase flow, in most currently used reactor safety analysis codes, is limited. Such flow regime maps are based on steady state, fully developed flow assumptions, which is an arguably poor assumption for reactor system transients. To improve this situation, it has been prosed that dynamical flow regime models be considered that are based, for example, on the interfacial area transport theory with regard for appropriate length and time scales. The RELAP-7 system code will certainly be improved with future incorporation of such dynamical flow regime models.

Future assessment of the RELAP-7 code is another critical task. This includes verification and validation and uncertainty quantification as outlined in the Light Water Reactor Sustainability (LWRS) Program verification and validation strategy document [13]. The assessment activities will necessarily span the entire intended application set of the code. Different types of experimental results need to be collected and reviewed. These include results from thought and analytical benchmark tests, separate effects tests, component tests, integral effects tests, and plant tests. Thought and analytical benchmark tests are simple tests where we know or can easily get the solution, even without a physical experiment being performed. Separate effects test results are used to validate and quantify uncertainty for single-physics models. Component test results are used to validate and calibrate key parameters in a physical component. Integral effects tests are performed on large-scale experiment facilities. These results can validate how well the code performs in modeling transients with a large number of phenomena. Plant tests and events are performed on real operating plants, including the Advanced Test Reactor. The results can validate how well the code can predict plant transient behavior. All tests in the RELAP5-3D developmental assessment package will be reviewed, along with additional tests used by other codes, such as the U.S. Nuclear Regulatory Commission code TRACE.

5. REFERENCES

1. Andrea Prosperetti and Grétar Tryggvason (Editors), "Computational Methods for Multiphase Flow (Chapter 11.6)," Cambridge University Press, 2007, 2009.
2. Ray A. Berry, Richard Saurel, and Olivier LeMetayer, "The discrete equation method (DEM) for fully compressible, two-phase flows in ducts of spatially varying cross-section," *Nuclear Engineering and Design*, 240 (2010), 3797–3818.
3. R. A. Berry, *Some Specific CASL Requirements for Advanced Multiphase Flow Simulations of Light Water Reactors*, Idaho National Laboratory, INL/EXT-10-20529, December 2010.
4. R. A. Berry (PI), R. Saurel, F. Petitpas, E. Daniel, O. LeMetayer, S. Gavrilyuk, N. Dovetta, and R. C. Martineau, *Progress in the Development of Compressible, Multiphase Flow Modeling Capability for Nuclear Reactor Flow Applications*, Idaho National Laboratory, INL/EXT-08-15002, October 2008.
5. *RELAP-7 Level 2 Milestone Report: Demonstration of a Steady State Single Phase PWR Simulation with RELAP-7*, Idaho National Laboratory, INL/EXT-12-25924, May 2012.
6. D. Gaston, C. Newman, G. Hansen, and D. Lebrun-Grandie: "MOOSE: A Parallel Computational Framework for Coupled Systems of Nonlinear Equations," *Nuclear Engineering and Design*, 239 (2009), 1768–1778.
7. R.A. Berry, "The Seven, Five, and Three-Equation Models of Compressible Two-Phase Flow: A Fully Consistent, Hierarchical Set," in preparation.
8. H. Stadtke, *Gasdynamic Aspects of Two-Phase Flow: Hyperbolicity, Wave Propagation Phenomena and Related Numerical Methods*, Wiley-VCH Verlag GmbH & Co, KGaA, Weinheim, Germany (2006).
9. R. A. Berry, "A Logical Progression of Steps for Implementation and Testing of the 7-Equation, Two-Phase Model into a Computational Framework," *International Conference on Mathematics and Computational Methods Applied to Nuclear Science & Engineering (M&C 2013)*, Sun Valley, Idaho, USA, May 5–9, 2013.
10. O. LeMetayer, J. Massoni, and R. Saurel, "Elaborating Equations of State of a Liquid and its Vapor for Two-Phase Models," *Int. J. Thermal Sciences*, 43, (2004), 265–276.
11. *RELAP5-3D Code Manual Volume 1: Code Structure, System Models and Solution Methods*, Idaho National Laboratory, INEEL-EXT-98-00834, June 2012.
12. "TRACE V5.0 Theory Manual, Field Equations, Solution Methods and Physical Model," U.S. NRC, http://pbadupws.nrc.gov/docs/ML0710/ML071000097.pdf.
13. C. Stoots, T. Larson, R. Schultz, H. Gougar, K. McCarthy, D. Petti, L. Swiler, M. Corradini, *Verification and Validation Strategy for LWRS* Tools, Idaho National Laboratory report INL/EXT-12-27066, September 2012.

Appendix A

A LOGICAL PROGRESSION OF STEPS FOR IMPLEMENTATION AND TESTING OF THE 7-EQUATION, TWO-PHASE MODEL INTO A COMPUTATIONAL FRAMEWORK

This appendix is a copy of an accepted paper from the upcoming American Nuclear Society conference: *International Conference on Mathematics and Computational Methods Applied to Nuclear Science & Engineering (M&C 2013)*, Sun Valley, Idaho, USA, May 5 - 9, 2013 (available from American Nuclear Society, LaGrange Park, IL).

International Conference on Mathematics and Computational Methods Applied to Nuclear Science & Engineering (M&C 2013), Sun Valley, Idaho, USA, May 5-9, 2013, on CD-ROM, American Nuclear Society, LaGrange Park, IL (2013)

A LOGICAL PROGRESSION OF STEPS FOR IMPLEMENTATION AND TESTING OF THE 7-EQUATION, TWO-PHASE MODEL INTO A COMPUTATIONAL FRAMEWORK

R. A. Berry*
Idaho National Laboratory
P.O. Box 1625, Idaho Falls, Idaho, USA 93415-3840
ray.berry@inl.gov

ABSTRACT

A seven-step progression is given for the implementation of the seven-equation model, employed in the new RELAP-7 thermal hydraulics system analysis code, within the MOOSE-compatible framework. The model is well-posed and treats both phases as compressible flow in a one-dimensional, variable cross-sectional area duct/pipe/component. Some appropriate tests are also outlined to benchmark the model/implementation for each step of the progression.

Key Words: RELAP-7, MOOSE, two-phase flow, 7-equation model, well-posed model

1. INTRODUCTION

For the simulation of nuclear reactor coolant flows general two-phase flow models which allow velocity disequilibrium, but which assume pressure equilibrium between the phases, are typically used (see Stadtke [1] for a recent review). These ill-posed equations are usually not hyperbolic, their physical wave dynamics are incorrect, and their solution algorithms rely on dubious properties (e.g. truncation error induced artificial viscosity) to render them numerically well-posed over a portion of the computational spectrum[1]. Thus these traditional models cannot achieve a grid-converged solution because the truncation error (artificial viscosity) becomes small, allowing the ill-posed artifacts of the model to dominate. Well-posed, hyperbolic models are important for transient flows.

The new RELAP-7 thermal hydraulics system analysis code, as well as companion multi-dimensional two-phase CFD codes under development at the Idaho National Laboratory (INL), employs a 7-equation, compressible, two-phase model that does not assume pressure equilibrium between the phases. This physically motivated (inviscid) model has real characteristics, is well-posed, and is hyperbolic. Both phases must be compressible to correctly handle wave

* Phone: +1 208 526 1254

[1] Numerical dissipation per se is not dubious. Nonlinear hyperbolic equation systems have solutions that always exhibit a propensity toward development of discontinuous behavior, so dissipation of varying level should always be present. The use of controlled artificial viscosity (as a physical regularization) to enforce an appropriate entropy condition and select a unique, physically meaningful, weak solution is well known. It is dubious, however, to use this mechanism to select a supposedly "physical solution" for a nonphysical, ill-posed system that is somehow arbitrarily close to the solution of a physical, well-posed, but *unknown* system.

propagation and bubble collapse, etc. For more details of this model the reader is referred to [2] and the references therein.

This 7-equation model is being implemented as a one-dimensional, variable cross-sectional area system within RELAP-7 using the INL MOOSE (Multiphysics, Object-Oriented, Simulation Environment) finite element framework [3]. This will allow strong, seamless coupling with a growing family of neutronics, heat conduction, and fuels performance codes all under development at the INL using the common MOOSE framework.

In this short note, the logical steps of progression are enumerated whereby the complicated 7-equation model is implemented within the MOOSE framework. This sequential progression is followed to allow physically- and numerically-meaningful, benchmark testing at each step in order to gain confidence in its correct implementation.

As this code is in the initial stages of development, results for simulations with this model will be given later.

2. SEVEN-STEP IMPLIMENTATION AND TESTING PROGRESSION

The following progression of step is designed to go successively from single-phase compressible flow in a duct of spatially varying cross-sectional area to a compressible, two-phase flow with full thermodynamic and mechanical nonequilibrium. Note that the cross-sectional area is carried inside the time-derivative for (possible) future inclusion of duct stretching (diameter) effects. Though only 1-D equations are shown here, the same step-progression could be employed for the multi-dimensional code implementation using the corresponding multi-dimensional descriptive equations.

Step 1

This first step tests only a single phase, compressible fluid utilizing the stiffened gas equation of state (SGEOS).

Mass, Momentum, and Total Energy Balance Equations

$$\frac{\partial \rho_l A}{\partial t} + \frac{\partial \rho_l u_l A}{\partial x} = 0$$

$$\frac{\partial \rho_l u_l A}{\partial t} + \frac{\partial A(\rho_l u_l^2 + p_l)}{\partial x} = p_l \frac{\partial A}{\partial x}$$

$$\frac{\partial \rho_l E_l A}{\partial t} + \frac{\partial u_l A(\rho_l E_l + p_l)}{\partial x} = 0$$

Stiffened Gas Equation of State (SGEOS)

$$e(p,\rho)=\frac{p+\gamma p_\infty}{(\gamma-1)\rho}+q \qquad e(\rho,T)=c_vT+q+\frac{p_\infty}{\rho} \qquad c_p=\gamma c_v$$

$$\rho(p,T)=\frac{p+p_\infty}{(\gamma-1)c_vT} \qquad c^2=\frac{\gamma(p+p_\infty)}{\rho}=\gamma(\gamma-1)c_vT$$

$$h(T)=\gamma c_vT+q \qquad s(p,T)=c_v\ln\frac{T^\gamma}{(p+p_\infty)^{(\gamma-1)}}+q'$$

$$g(p,T)=h(T)-Ts(p,T)=(\gamma c_v-q')T-c_vT\ln\frac{T^\gamma}{(p+p_\infty)^{(\gamma-1)}}+q$$

This equation of state can represent a compressible gas or a compressible liquid and will be used in the next step. Even though the PDE's for this step show a "liquid" subscript, they are equally applicable for gas or vapor, and indeed for this step, single-phase compressible flow should be demonstrated for both gas and for liquid with appropriate parameters in the SGEOS (as given in step 2).

Some appropriate benchmark tests for step 1 should include the following (for each phase!):

1. Set $u=0$, and $p=uniform\,(\rho=uniform, e=uniform)$. Set an arbitrarily severe cross-sectional area distribution to get corresponding $\partial A/\partial x$. Integrate over time. No changes should occur, especially in velocity, i.e. the acceleration should be zero. Also check the $\rho, u, and\ E$ distributions; they shouldn't change either.
2. Test boundary conditions.
3. Test for low Mach number issues (poor spatial accuracy for flows with $0 < Mach < 0.3$).
4. Set uniform *u*, uniform *p*, and uniform *A*. Set appropriate boundary conditions. Prescribe a ρ spatial distribution (e.g. a step). With time the ρ distribution should undergo simple advection (linearly with velocity). Both *p* and *u* should remain uniform.

Step2

In this step, another compressible fluid is added. No interaction is included, except a common mesh and time step -- just two independent, simultaneous problems, to provide an initial test of the system solver for the enlarged system. The equations added for this step (from those of step 1 above) are shown in red.

Liquid

$$\frac{\partial\rho_lA}{\partial t}+\frac{\partial\rho_lu_lA}{\partial x}=0$$

$$\frac{\partial \rho_l u_l A}{\partial t} + \frac{\partial A(\rho_l u_l^2 + p_l)}{\partial x} = p_l \frac{\partial A}{\partial x}$$

$$\frac{\partial \rho_l E_l A}{\partial t} + \frac{\partial u_l A(\rho_l E_l + p_l)}{\partial x} = 0$$

Vapor

$$\frac{\partial \rho_g A}{\partial t} + \frac{\partial \rho_g u_g A}{\partial x} = 0$$

$$\frac{\partial \rho_g u_g A}{\partial t} + \frac{\partial A(\rho_g u_g^2 + p_g)}{\partial x} = p_g \frac{\partial A}{\partial x}$$

$$\frac{\partial \rho_g E_g A}{\partial t} + \frac{\partial u_g A(\rho_g E_g + p_g)}{\partial x} = 0$$

with the SGEOS parameters of ***Table I*** as follows.

Table I. Stiffened gas equation of state parameters for water and its vapor [4]

Water	γ_k	$q_k \left(J \cdot kg^{-1}\right)$	$q_k' \left(J \cdot kg^{-1} \cdot K^{-1}\right)$	$p_{\infty k} \left(Pa\right)$	$c_{vk} \left(J \cdot kg^{-1} \cdot K^{-1}\right)$
Liquid	2.35	$-1167 \cdot 10^3$	0	10^9	1816
Vapor	1.43	$2030 \cdot 10^3$	$-23 \cdot 10^3$	0	1040

A basic test to run for step 2 is to verify that, with identical boundary conditions for both systems (phases) that all of the results of step 1 are obtained efficiently. After all, there is no interaction between the phases.

Step 3

For this step, volume fraction effects are added (in red). This is, the independent phases share the flow volume of the variable cross-sectional area duct, but otherwise have no interaction.

Liquid

$$\frac{\partial \alpha_l \rho_l A}{\partial t} + \frac{\partial \alpha_l \rho_l u_l A}{\partial x} = 0$$

$$\frac{\partial \alpha_l \rho_l u_l A}{\partial t} + \frac{\partial \alpha_l A(\rho_l u_l^2 + p_l)}{\partial x} = p_l \alpha_l \frac{\partial A}{\partial x} + p_l A \frac{\partial \alpha_l}{\partial x}$$

$$\frac{\partial \alpha_l \rho_l E_l A}{\partial t} + \frac{\partial \alpha_l u_l A(\rho_l E_l + p_l)}{\partial x} = 0$$

$$\alpha_l(x) \text{ specified}, \quad 0 < \alpha_l(x) < 1$$

Vapor

$$\frac{\partial \alpha_g \rho_g A}{\partial t} + \frac{\partial \alpha_g \rho_g u_g A}{\partial x} = 0$$

$$\frac{\partial \alpha_g \rho_g u_g A}{\partial t} + \frac{\partial \alpha_g A(\rho_g u_g^2 + p_g)}{\partial x} = p_g \alpha_g \frac{\partial A}{\partial x} + p_g A \frac{\partial \alpha_g}{\partial x}$$

$$\frac{\partial \alpha_g \rho_g E_g A}{\partial t} + \frac{\partial \alpha_g u_g A(\rho_g E_g + p_g)}{\partial x} = 0$$

$$\alpha_g(x) = 1 - \alpha_l(x)$$

Basic tests for step 3 should include the following:

1. Make A uniform, but give α an arbitrarily severe spatial distribution (e.g. the normalized version of that for $\partial A/\partial x$ of problem 1 of step 1. The solutions should be identical to the corresponding $\partial A/\partial x$ case with single phase (no α).
2. Test boundary conditions for α.
3. Set $p_g = p_l$ *and uniform*. Also set ρ_g *and* ρ_l *uniform* as well as $u_g = u_l$ *and uniform*. Set A uniform and prescribe an arbitrary α spatial distribution. Set appropriate boundary conditions. With time evolution, α should simply advect linearly with velocity.

Step 4

In this step, a fully two-phase is achieved, with phase interaction but no relaxation or phase change. Additional or modified terms (from the previous step) are shown in red.

Liquid

$$\frac{\partial \alpha_l A}{\partial t} + u_{\text{int}} A \frac{\partial \alpha_l}{\partial x} = 0$$

$$\frac{\partial \alpha_l \rho_l A}{\partial t} + \frac{\partial \alpha_l \rho_l u_l A}{\partial x} = 0$$

$$\frac{\partial \alpha_l \rho_l u_l A}{\partial t} + \frac{\partial \alpha_l A(\rho_l u_l^2 + p_l)}{\partial x} = p_l \alpha_l \frac{\partial A}{\partial x} + p_{\text{int}} A \frac{\partial \alpha_l}{\partial x}$$

$$\frac{\partial \alpha_l \rho_l E_l A}{\partial t} + \frac{\partial \alpha_l u_l A(\rho_l E_l + p_l)}{\partial x} = p_{\text{int}} u_{\text{int}} A \frac{\partial \alpha_l}{\partial x}$$

Vapor

$$\frac{\partial \alpha_g A}{\partial t} + u_{\text{int}} A \frac{\partial \alpha_g}{\partial x} = 0 \qquad \left(\textit{not needed for two phases}, \alpha_g = 1 - \alpha_l \right)$$

$$\frac{\partial \alpha_g \rho_g A}{\partial t} + \frac{\partial \alpha_g \rho_g u_g A}{\partial x} = 0$$

$$\frac{\partial \alpha_g \rho_g u_g A}{\partial t} + \frac{\partial \alpha_g A(\rho_g u_g^2 + p_g)}{\partial x} = p_g \alpha_g \frac{\partial A}{\partial x} + p_{\text{int}} A \frac{\partial \alpha_g}{\partial x}$$

$$\frac{\partial \alpha_g \rho_g E_g A}{\partial t} + \frac{\partial \alpha_g u_g A(\rho_g E_g + p_g)}{\partial x} = p_{\text{int}} u_{\text{int}} A \frac{\partial \alpha_g}{\partial x}$$

where the interfacial variables are

$$u_{\text{int}} = \bar{u}_{\text{int}} + \text{sgn}\left(\frac{\partial \alpha_l}{\partial x} \right) \frac{p_g - p_l}{Z_l + Z_g}, \qquad \bar{u}_{\text{int}} = \frac{Z_l u_l + Z_g u_g}{Z_l + Z_g}$$

$$p_{\text{int}} = \bar{p}_{\text{int}} + \frac{Z_l Z_g}{Z_l + Z_g} \text{sgn}\left(\frac{\partial \alpha_l}{\partial x} \right) \cdot (u_g - u_l), \qquad \bar{p}_{\text{int}} = \frac{Z_g p_l + Z_l p_g}{Z_l + Z_g} \quad .$$

where $Z_k = \rho_k c_k \left(k = g, l \right)$ is the phasic acoustic impedance (where c_k is the phasic sound speed). These variables correspond to the interface velocity of, and pressure exerted on, the surface of a two-phase control volume, i.e. at locations where volume fraction gradients are present. The quantities with the over-bar indicate average interfacial velocity and pressure acting inside the two-phase control volume.

For step 4 a good benchmark test is to set a uniform α_k spatial distribution along with appropriate boundary conditions. Solutions should be the same as those for step 2. Again it is crucial to repeat test 3 of step 3.

Step 5

In this step, velocity-relaxation (blue) and pressure-relaxation (red) terms are added:

Liquid

$$\frac{\partial \alpha_l A}{\partial t} + u_{\text{int}} A \frac{\partial \alpha_l}{\partial x} = A\mu(p_l - p_g)$$

$$\frac{\partial \alpha_l \rho_l A}{\partial t} + \frac{\partial \alpha_l \rho_l u_l A}{\partial x} = 0$$

$$\frac{\partial \alpha_l \rho_l u_l A}{\partial t} + \frac{\partial \alpha_l A(\rho_l u_l^2 + p_l)}{\partial x} = p_l \alpha_l \frac{\partial A}{\partial x} + p_{\text{int}} A \frac{\partial \alpha_l}{\partial x} + A\lambda(u_g - u_l)$$

$$\frac{\partial \alpha_l \rho_l E_l A}{\partial t} + \frac{\partial \alpha_l u_l A(\rho_l E_l + p_l)}{\partial x} = p_{\text{int}} u_{\text{int}} A \frac{\partial \alpha_l}{\partial x} - \overline{p}_{\text{int}} A\mu(p_l - p_g) + \overline{u}_{\text{int}} A\lambda(u_g - u_l)$$

Vapor

$$\frac{\partial \alpha_g A}{\partial t} + u_{\text{int}} A \frac{\partial \alpha_g}{\partial x} = A\mu(p_g - p_l) \qquad \left(\textit{not needed for two phases}, \alpha_g = 1 - \alpha_l\right)$$

$$\frac{\partial \alpha_g \rho_g A}{\partial t} + \frac{\partial \alpha_g \rho_g u_g A}{\partial x} = 0$$

$$\frac{\partial \alpha_g \rho_g u_g A}{\partial t} + \frac{\partial \alpha_g A(\rho_g u_g^2 + p_g)}{\partial x} = p_g \alpha_g \frac{\partial A}{\partial x} + p_{\text{int}} A \frac{\partial \alpha_g}{\partial x} + A\lambda(u_l - u_g)$$

$$\frac{\partial \alpha_g \rho_g E_g A}{\partial t} + \frac{\partial \alpha_g u_g A(\rho_g E_g + p_g)}{\partial x} = p_{\text{int}} u_{\text{int}} A \frac{\partial \alpha_g}{\partial x} - \overline{p}_{\text{int}} A\mu(p_g - p_l) + \overline{u}_{\text{int}} A\lambda(u_l - u_g)$$

where mechanical non-equilibrium is represented with a relaxation process whose rate is controlled by the following *mechanical relaxation parameters*:

$$\lambda = \frac{1}{2}\mu Z_l Z_g \quad \text{(velocity relaxation rate)}$$

$$\mu = \frac{A_{\text{int}}}{Z_l + Z_g} \quad \text{(pressure relaxation rate),}$$

where A_{int} represents the specific interfacial area; again Z_k is the phasic acoustic impedance.

An important test for step 5 is to set the α spatial distribution uniform. Set the mechanical relaxation coefficients $\mu = 0$ *and* $\lambda = 0$. Again the solution results should match those of step 2. Another crucial test for this step is again that of test 3 of step 3.

Step 6

Interfacial mass transfer (red) effects and direct interfacial heat transfer (blue) are added in this step as follows:

Liquid

$$\frac{\partial \alpha_l A}{\partial t} + u_{\text{int}} A \frac{\partial \alpha_l}{\partial x} = A\mu(p_l - p_g) - \frac{\Gamma A_{\text{int}} A}{\rho_{\text{int}}}$$

$$\frac{\partial \alpha_l \rho_l A}{\partial t} + \frac{\partial \alpha_l \rho_l u_l A}{\partial x} = -\Gamma A_{\text{int}} A$$

$$\frac{\partial \alpha_l \rho_l u_l A}{\partial t} + \frac{\partial \alpha_l A(\rho_l u_l^2 + p_l)}{\partial x} = p_{\text{int}} A \frac{\partial \alpha_l}{\partial x} + p_l \alpha_l \frac{\partial A}{\partial x} + A\lambda(u_g - u_l) - \Gamma A_{\text{int}} u_{\text{int}} A$$

$$\frac{\partial \alpha_l \rho_l E_l A}{\partial t} + \frac{\partial \alpha_l u_l A(\rho_l E_l + p_l)}{\partial x} = p_{\text{int}} u_{\text{int}} A \frac{\partial \alpha_l}{\partial x} - \bar{p}_{\text{int}} A\mu(p_l - p_g) + \bar{u}_{\text{int}} A\lambda(u_g - u_l) + \Gamma A_{\text{int}} \left(\frac{p_{\text{int}}}{\rho_{\text{int}}} - H_{l\,\text{int}} \right) A + A_{\text{int}} h_{Tl}(T_{\text{int}} - T_l) A$$

Vapor

$$\frac{\partial \alpha_g A}{\partial t} + u_{\text{int}} A \frac{\partial \alpha_g}{\partial x} = A\mu(p_g - p_l) + \frac{\Gamma A_{\text{int}} A}{\rho_{\text{int}}} \qquad \left(\textit{not needed for two phases}, \alpha_g = 1 - \alpha_l \right)$$

$$\frac{\partial \alpha_g \rho_g A}{\partial t} + \frac{\partial \alpha_g \rho_g u_g A}{\partial x} = \Gamma A_{\text{int}} A$$

$$\frac{\partial \alpha_g \rho_g u_g A}{\partial t} + \frac{\partial \alpha_g A(\rho_g u_g^2 + p_g)}{\partial x} = p_{\text{int}} A \frac{\partial \alpha_g}{\partial x} + p_g \alpha_g \frac{\partial A}{\partial x} + A\lambda(u_l - u_g) + \Gamma A_{\text{int}} u_{\text{int}} A$$

$$\frac{\partial \alpha_g \rho_g E_g A}{\partial t} + \frac{\partial \alpha_g u_g A(\rho_g E_g + p_g)}{\partial x} = p_{\text{int}} u_{\text{int}} A \frac{\partial \alpha_g}{\partial x} - \overline{p}_{\text{int}} A \mu (p_g - p_l)$$
$$+ \overline{u}_{\text{int}} A \lambda (u_l - u_g) - \Gamma A_{\text{int}} \left(\frac{p_{\text{int}}}{\rho_{\text{int}}} - H_{g\,\text{int}} \right) A + A_{\text{int}} h_{Tg} (T_{\text{int}} - T_g) A$$

This system is unconditionally ***hyperbolic*** and admits the characteristic wave speeds $u_k + c_k$, $u_k - c_k$, u_k for each phase k, along with the interface velocity u_I. For additional details of nomenclature, phase change models, boundary conditions, and other needed closure relations, refer to [2].

For all of the steps 1 through 6, in addition to the prescribed tests above, we have relied significantly on the known analytical solutions for compressible flow in converging-diverging nozzles with stagnation inlet boundary condition and static pressure outlet boundary condition. This solution is known for slow flows, fast flows, and flows with shocks for stiffened gas equation of state, and therefore applies to both the gas and liquid flows (see e.g. [2, 5]). The low velocity version provides an excellent benchmark test of the algorithms ability to accurately and efficiently solve low Mach number compressible flows. Note however, when mechanical and/or thermal relaxation terms are active then the nonlinear solutions are not know; only the special cases with non-active relaxation. But that gives confidence in the algorithms ability to compute these special limiting cases with the same nonlinear algorithm.

Step 7

Finally, gravity force (magenta), wall and interphase viscous drag (red), and simple wall heat transfer (no phase change induced directly at the wall) (blue) are added to the model.

Liquid

$$\frac{\partial \alpha_l A}{\partial t} + u_{\text{int}} A \frac{\partial \alpha_l}{\partial x} = A \mu (p_l - p_g) - \frac{\Gamma A_{\text{int}} A}{\rho_{\text{int}}}$$

$$\frac{\partial \alpha_l \rho_l A}{\partial t} + \frac{\partial \alpha_l \rho_l u_l A}{\partial x} = -\Gamma A_{\text{int}} A$$

$$\frac{\partial \alpha_l \rho_l u_l A}{\partial t} + \frac{\partial \alpha_l A(\rho_l u_l^2 + p_l)}{\partial x} = p_{\text{int}} A \frac{\partial \alpha_l}{\partial x} + p_l \alpha_l \frac{\partial A}{\partial x} + A \lambda (u_g - u_l) - \Gamma A_{\text{int}} u_{\text{int}} A$$
$$- f_l \alpha_l \rho_l \left(u_l - u_w \right)^2 (\pi A)^{\frac{1}{2}} - f_l' \tfrac{1}{2} \rho_l \left(u_l - u_{\text{int}} \right)^2 A_{\text{int}} A + \alpha_l \rho_l \vec{g} \cdot \hat{n}_{axis} A$$

$$\frac{\partial \alpha_l \rho_l E_l A}{\partial t} + \frac{\partial \alpha_l u_l A(\rho_l E_l + p_l)}{\partial x} = p_{\text{int}} u_{\text{int}} A \frac{\partial \alpha_l}{\partial x} - \bar{p}_{\text{int}} A \mu (p_l - p_g)$$
$$+ \bar{u}_{\text{int}} A \lambda (u_g - u_l) + \Gamma A_{\text{int}} \left(\frac{p_{\text{int}}}{\rho_{\text{int}}} - H_{l\,\text{int}} \right) A + A_{\text{int}} h_{Tl} (T_{\text{int}} - T_l) A$$
$$+ \alpha_l h_{lw} (T_w - T_l) \left[4\pi A + \left(\frac{\partial A}{\partial x} \right)^2 \right]^{\frac{1}{2}} + \alpha_l \rho_l u_l \vec{g} \cdot \hat{n}_{axis} A$$

Vapor

$$\frac{\partial \alpha_g A}{\partial t} + u_{\text{int}} A \frac{\partial \alpha_g}{\partial x} = A \mu (p_g - p_l) + \frac{\Gamma A_{\text{int}} A}{\rho_{\text{int}}} \qquad \left(\textit{not needed for two phases, } \alpha_g = 1 - \alpha_l \right)$$

$$\frac{\partial \alpha_g \rho_g A}{\partial t} + \frac{\partial \alpha_g \rho_g u_g A}{\partial x} = \Gamma A_{\text{int}} A$$

$$\frac{\partial \alpha_g \rho_g u_g A}{\partial t} + \frac{\partial \alpha_g A(\rho_g u_g^2 + p_g)}{\partial x} = p_{\text{int}} A \frac{\partial \alpha_g}{\partial x} + p_g \alpha_g \frac{\partial A}{\partial x} + A \lambda (u_l - u_g) + \Gamma A_{\text{int}} u_{\text{int}} A$$
$$- f_g \alpha_g \rho_g \left(u_g - u_w \right)^2 (\pi A)^{\frac{1}{2}} - f_g' \tfrac{1}{2} \rho_g \left(u_g - u_{\text{int}} \right)^2 A_{\text{int}} A + \alpha_g \rho_g \vec{g} \cdot \hat{n}_{axis} A$$

$$\frac{\partial \alpha_g \rho_g E_g A}{\partial t} + \frac{\partial \alpha_g u_g A(\rho_g E_g + p_g)}{\partial x} = p_{\text{int}} u_{\text{int}} A \frac{\partial \alpha_g}{\partial x} - \bar{p}_{\text{int}} A \mu (p_g - p_l)$$
$$+ \bar{u}_{\text{int}} A \lambda (u_l - u_g) - \Gamma A_{\text{int}} \left(\frac{p_{\text{int}}}{\rho_{\text{int}}} - H_{g\,\text{int}} \right) A + A_{\text{int}} h_{Tg} (T_{\text{int}} - T_g) A$$
$$+ \alpha_g h_{gw} (T_w - T_g) \left[4\pi A + \left(\frac{\partial A}{\partial x} \right)^2 \right]^{\frac{1}{2}} + \alpha_g \rho_g u_g \vec{g} \cdot \hat{n}_{axis} A$$

Simple benchmark tests for step 7 should include both wall friction and simple heat addition induced choking.

3. CONCLUSIONS

A logical and sequential progression of steps has been presented for the implementation of the advanced 7-equation compressible two-phase flow model within a modern computational framework, the INL MOOSE framework. The steps allow for intermediate benchmark testing

against known solutions, some of which are also specified, so the complexity can be confidently increased in a step-wise manner.

ACKNOWLEDGMENTS

The author acknowledges the US Department of Energy, Office of Nuclear Energy, for funding this research at the Idaho National Laboratory under DOE Idaho Operations Office Contract DE-AC07-05ID14517.

REFERENCES

1. H. Stadtke, *Gasdynamic Aspects of Two-Phase Flow: Hyperbolicity,, Wave Propagation Phenomena and Related Numerical Methods*, Wiley-VCH Verlag GmbH & Co, KGaA, Weinheim, Germany (2006).
2. R.A. Berry, R. Saurel, and O. LeMetayer, "The discrete equation method (DEM) for fully compressible, two-phase flows in ducts of spatially varying cross-section," *Nuclear Engineering and Design* **240**, pp. 3797-3818 (2010).
3. D. Gaston, C. Newman, G. Hansen, and D. Lebrun-Grandie, "MOOSE: A Parallel Computational Framework for Coupled Systems of Nonlinear Equations," *Nuclear Engineering and Design* **239**, pp. 1768-1778 (2009).
4. O. LeMetayer, J. Massoni, and R. Saurel, "Elaborating equations of state of a liquid and its vapor for two-phase flow models," *Int. J. Thermal Sciences* **43**, pp. 265-276 (2004) [in French].
5. S.Y. Kadioglu, R.A. Berry, and R.C. Martineau, "A Point Implicit Time Integration Technique for Slow Transient Flow Problems," *Nuclear Engineering and Design*, submitted 2012.